Xanthohumol as a potential therapeutic strategy for acute myeloid leukemia: Targeting the FLT3/SRPK1 signaling axis

Duan-Na Zhang [a], Wen-Ya Yang [a], Xiao-Xue Hu [a], Xiao-Min-Ting Song [a,b], Chuan-Jie Guo [a,c], Fu Peng [d], Yu-Zhi Li [a,**], Zhi-Xing Cao [a,*]

[a] The State Key Laboratory of Southwest Chinese Medicine Resources, School of Pharmacy, Chengdu University of Traditional Chinese Medicine, Chengdu, 611137, China
[b] State Key Laboratory Breeding Base of Systematic Research, Development and Utilization of Chinese Medicine Resources, Chengdu University of Traditional Chinese Medicine, Chengdu 611137, China
[c] School of Basic Medicine, Chengdu University of Traditional Chinese Medicine, Chengdu, 610075, China
[d] West China School of Pharmacy, State Key Laboratory of Biotherapy, West China Hospital, Sichuan University, Chengdu, 610041, China

Abstract

Xanthohumol (XN) is an isoprene chalcone found in hops (*Humulus lupulus L.*), a food ingredient with a wide range of pharmacological activities. The aim of this study was to reveal the therapeutic effect of XN on acute myeloid leukemia (AML) and the potential underlying molecular mechanism. Through network pharmacology analysis, molecular docking, and HTRF determination, XN was shown to inhibit the kinase activities of FLT3 and SRPK1 by targeting their ATP-binding domains, with IC_{50} values of 1.51 ± 0.44 μM and 0.37 ± 0.15 μM, respectively. By inhibiting AML cell proliferation, promoting apoptosis, regulating autophagy, and inhibiting invasion, XN, which targets the unique FLT3/SRPK1 signaling pathway, exerts anti-AML effects. XN also significantly inhibited FLT3 inhibitor-resistant AML cells and exhibited synergistic interactions with gilteritinib. Moreover, XN at 40 mg/kg effectively inhibited the growth of AML subcutaneous tumors with good tolerance. These results suggest that XN could be a promising therapeutic agent for AML treatment. XN effectively targets the FLT3/SRPK1 signaling axis, demonstrating strong anti-AML effects and offering a potent strategy to address AML.

Keywords: Acute myeloid leukemia, Apoptosis, FLT3/SRPK1, Xanthohumol

1. Introduction

Acute myeloid leukemia (AML) is a highly malignant illness affecting the hematological system. Mutations in the class III receptor tyrosine kinase FLT3, which regulates hematopoiesis, are key promoters of AML and often occur in approximately 30% of adult AML patients. Mutated FLT3 promotes unrestricted growth of AML cells by continuously activating downstream signaling pathways such as the AKT/mTOR and ERK/cMYC pathways [1]. FLT3 inhibitors have successfully delayed the progression of FLT3-mutant AML patients in clinical practice. However, multiple mutations and heterogeneity in AML cells can easily lead to drug resistance. The long-term use of single-target drugs is prone to rapid recurrence due to drug resistance, which cannot achieve long-term clinical efficacy [2]. Therefore, multitarget treatment or combined treatment is highly important for improving the prognosis of AML patients and reversing drug resistance. SRPK1 is an important subtype of the serine arginine (SR) protein kinase family. By regulating splicing factors, SRPK1 plays an

Received 30 April 2024; accepted 4 October 2024.
Available online 31 March 2025

* Corresponding author.
** Corresponding author.
E-mail addresses: liyuzhi@cdutcm.edu.cn (Y.-Z. Li), caozhixing@cdutcm.edu.cn (Z.-X. Cao).

https://doi.org/10.38212/2224-6614.3534

important role in promoting cell transcription, mRNA transport, and protein translation and participates in promoting the cell cycle process, cell proliferation, and migration in a variety of physiological processes [3,4]. Abnormal expression of SRPK1 and changes in its function can promote tumorigenesis. Dysregulation or overexpression of SRPK1 is beneficial for the growth and proliferation of chronic myeloid leukemia (CML), adult T-cell leukemia (ATL), and acute lymphoblastic leukemia (ALL) cells [5–7]. Recently, SRPK1 was identified as a potential therapeutic strategy for AML through the CRISPR Dropout Screen [8], and silencing SRPK1 expression can alter the level of the key protein short bromodomain 4 (BRD4), which is involved in the expulsion of BCL2 and cMYC, all of which exert antihuman acute myeloid leukemia effects [9]. In summary, SRPK1 is a novel drug therapeutic target for AML treatment.

Xanthohumol (XN) is found primarily in the female inflorescence of Hop plants, which are scientifically known as *Humulus lupulus L*. In 1913, XN was first isolated from hops and named by Power et al. [10]. In 1957, it was not until Verzele joined that the chemical structure of XN was ultimately determined, and XN was shown to be an isoprenyl chalcone [11]. In recent years, XN has been gradually applied in food, alcohol manufacturing, the sugar industry, and the pharmaceutical industry. XN has a diverse range of biological activities, including anti-inflammatory, antioxidative, anticancer, and additional pharmacological activities [12–14]. Studies have shown that XN can promote the apoptosis of chronic lymphocytic leukemia cells by inhibiting Bcl-2 and mcl-1 and by inducing caspase 9 [15]; exert anti-multiple myeloma effects *in vitro* by activating MAPK (ERK and JNK) [16]; and impair cell migration and invasion in acute lymphoblastic leukemia (ALL) cell lines by decreasing the crucial activation of the NF-κB, FAK, and AKT signaling pathways [17]. However, the efficacy of XN in AML and the underlying mechanism are still unclear.

In our previous studies, the therapeutic effect of XN on AML and its related potential molecular mechanism were investigated. Notably, we first detected XN as a natural AML inhibitor of FLT3/SRPK1. The effects of XN on the phosphorylation and activation of the kinases FLT3 and SRPK1, as well as its inhibitory effect on the FLT3/SRPK1 signaling cascade, were confirmed. In addition, the inhibitory activity of XN on FLT3 inhibitor-resistant cells and its anti-AML activity *in vivo* revealed the potential application value of FLT3/SRPK1 dual-target inhibitors. Overall, our data indicate that XN is an excellent lead drug for inhibiting the FLT3/SRPK1 axis, which provides a potential drug development strategy and experimental reference for the treatment of AML.

2. Materials and methods

2.1. Reagents

XN (CAS No. 6754-58-1, 99.95% purity) was purchased from Spring & Autumn (China); SPHINX31 (CAS No. 1818389-84-2, 99.13% purity) was obtained from MedChemExpress (MCE) (USA). Gilteritinib (CAS No. 6754-58-1, 98.97% purity) was purchased from BidePharmatech Co., Ltd. (China). DMSO and MTT were purchased from Sigma–Aldrich (USA) and BioFROXX (Germany), respectively. All drugs were dissolved in DMSO and diluted to the final concentration in fresh bath solution before each experiment. The drug solutions remained stable under light-protected conditions at 4 °C. A monodansylcadaverine (MDC) kit was purchased from Solarbio Science & Technology Co., Ltd. (China). 2-Hydroxypropyl-β-cyclodextrin was purchased from Beijing Biodee Biotechnology Co., Ltd. (China).

2.2. Cell culture

All the cell lines were maintained in their own media supplemented with 10% FBS (PAN-Biotech, Germany) and 1% penicillin/streptomycin (Invitrogen, USA) in 5% CO_2 at 37 °C. Specific media included RPMI-1640 for MOLM-13, H1299, RT4, and ASPC-1; DMEM for A-549, HELA, HEPA1-6, MDA-MB-453, and A2780; McCoy's 5A for HCT116 and SK-OV-3; IMDM for MV4-11; and MEM for MRC-5. The cells were passaged at 80–90% confluency and monitored daily with an inverted microscope. The media were changed every 1–2 days. The cell lines were obtained from the American Type Culture Collection (Manassas, VA, USA). Additionally, the cell lines used were free from cross-contamination or noncross-contamination and tested negative for mycoplasma contamination. All cells were authenticated through STR profiling, confirming a 100% match with the ATCC database.
(https://www.atcc.org/Products/All/CRL-3271.aspx#specifications).

2.3. Cell proliferation assay

Cells in the logarithmic phase of growth were seeded in 96-well plates at a density of 3×10^3 (adherent cells) or 3×10^4 cells/well (suspended

cells), and a control group was established. After 72 h of drug treatment, 20 μL of 5 g/L MTT solution was added to determine cell proliferation. Once blue formazan crystals formed, DMSO was added to dissolve the crystals, and the optical density (OD) was measured at 570 nm.

2.4. Bioinformatics analysis

The Swiss Target Prediction tool (http://www.swisstargetprediction.ch) was used to predict the active constituents of XN and their related targets. Screening for AML-related targets was performed via the GeneCards database (http://www.genecards.org) and the OMIM database (https://www.ncbi.nlm.nih.gov/omim/). The overlapping genes between XN and AML target genes were identified and visualized via a Venn diagram. Then, the drug-disease composite target network was constructed with the STRING database (https://string-db.org/) and Cytoscape software (https://cytoscape.org/). The DAVID v6.7 (https://www.david.ncifcrf.gov/) database was used for GO functional enrichment analysis and KEGG signaling pathway enrichment analysis. The $\chi 2$ test and Fisher's exact test for GO category classification were considered significant if $p < 0.05$ and FDR < 0.05 following correction for multiple comparisons. AutoDockTools-1.5.6 was used for molecular docking to verify the interactions between XN components and key target proteins. All the ligand molecules were drawn via ChemDraw 22.2.0, with the 2D structure of the XN molecule displayed. Energy minimization was performed via the MM2 force field in Chem3D Pro software. The receptor structure was obtained from the Protein Data Bank (PDB) (http://www.rcsb.org/). Finally, the molecular docking simulation diagram was constructed via PyMOL software.

2.5. In vitro kinase assay

An HTRF KinEASE-STK TM/TK Kit (Cisbio, France) was used to measure kinase inhibitory activity via an HTRF assay. The test compound was added to a 384-well plate, after which 2 μL of FLT3 or SRPK1 kinase (1 ng/μL) was added. The mixture was then coincubated with 4 μL of the test derivative. Then, 2 μL of TK substrate (1 μM) and 2 μL of ATP (0.1 μM) were added to initiate the reaction, and the reaction was stopped by adding EDTA detection solution. Finally, the TR-FRET signal was read by a VICTOR multilabel microplate detector (Perkin Elmer, Waltham, MA, USA) to determine the rate of inhibition and calculate the IC_{50}.

2.6. Western blotting

Log-phase MOLM-3 cells were treated with XN (5, 10, or 20 μM), SPHINX31 (5 μM), or gilteritinib (100 nM) for 24 h. Total protein was extracted via lysis buffer with protease and phosphatase inhibitors (RIPA: PMSF: cocktail = 1 mL: 13 μL: 10 μL). The protein concentration was measured via a BCA protein assay kit (Beyotime, China). Additionally, cells were treated with 20 μM XN and collected at different time points (0, 4, and 8 h) to extract cellular protein as previously described to analyze the dynamics of signaling pathway activation. The samples were mixed with loading buffer (Biosharp, China), and the proteins were denatured by heating. For electrophoretic protein separation, 10% or 15% gradient SDS–PAGE gels were prepared via an SDS–PAGE gel (Epizyme, Shanghai). Next, 10 μL of each denatured protein sample was loaded onto a gel for SDS–PAGE separation, after which the proteins were transferred to a PVDF membrane. After incubation with primary antibodies at 4 °C overnight, the membranes were subsequently incubated with secondary antibodies conjugated with HRP. The bands were subsequently detected via an ECL ultrasensitive substrate kit (Abbkine, China). After the phosphorylated protein was developed, stripping buffer was used to strip the membrane, after which total protein was detected at the same position; this ensures that both the phosphorylated protein and the total protein results are displayed on the same film simultaneously. The total and phosphorylated protein levels were quantified via ImageJ software (ImageJ 1.48v, NIH). Antibodies against AKT (A17909, 1:2500), p-AKT (AP0098, 1:500), BAX (A19684, 1:1000), BCL2 (A20777, 1:1000), and NF-κB (A11160, 1:500) were obtained from ABclonal. Antibodies against p-mTOR (2971S, 1:1000), mTOR (2983S, 1:1000), p-FLT3 (3464S, 1:1000), FLT3 (3462S, 1:1000) and cMYC (13987T, 1:1000) were obtained from Cell Signaling Technology. The antibodies against p-ERK (MA8131, 1:1000), ERK (T40071, 1:1000), p-SRPK1 (TA8457, 1:1000), SRPK1 (PU763328, 1:1000) and BRD4 (TD2905, 1:1000) were obtained from Abmart. Tumor tissues were excised from the mice, frozen in liquid nitrogen, and stored at −80 °C. A 100 mg sample was pulverized in a liquid nitrogen-cooled mortar and pestle. The powder was lysed in 1 mL of RIPA buffer supplemented with protease inhibitors and then sonicated at 70 Hz for 180 s. After centrifugation at 12,000 rpm for 15 min at 4 °C, the supernatant was collected. The remaining steps were performed as previously described.

2.7. Hoechst 33258 fluorescence staining

MOLM-13 cells were treated with XN (2.5, 5, or 10 μM), gilteritinib (1 μM), or SPHINX31 (5 μM) in 6-well plates for 48 h, and a control group was included for comparison. The cells were stained with a Hoechst-33258 kit (Beyotime, China) via incubation in 0.5 mL of Hoechst-33258 solution (10 μg/mL) for 10 min at room temperature. After staining, the cells were washed twice with PBS, centrifuged at 300×*g* for 3 min, and resuspended in 100 μL of PBS. A total of 20 μL samples were taken under a fluorescence microscope, the cells were observed, and fluorescence images were captured at excitation and emission wavelengths of 350 nm and 460 nm, respectively.

2.8. Cell apoptosis assay and cell cycle analysis

For the apoptosis assay, 5×10^5 MOLM-13 cells were seeded in 6-well plates and treated with XN (2.5, 5, or 10 μM), gilteritinib (1 μM), or SPHINX31 (5 μM) for 48 h. After the treatment, the samples were collected. The samples were incubated at a constant temperature for 15 min, as indicated by the V-FITC/PI apoptosis kit (Beyotime, China). For cell cycle analysis, the treated cells were collected, fixed overnight with 70% ethanol, and stained with PI staining buffer for 30 min at 37 °C in the dark. After staining, data were collected via a FACSVerse™ flow cytometer (BD Biosciences, USA), and at least 10,000 cells per sample were counted and analyzed with FlowJo 9.5.2 software.

2.9. Transmission electron microscopy

A total of 2×10^6 MOLM-13 cells in the logarithmic phase of growth were treated with 10 μM XN for 16 h, and a control group was established. The cells were fixed overnight with 2.5% glutaraldehyde at 4 °C, rinsed, and incubated for 2 h with 1% osmium tetroxide. Each sample underwent dehydration through a gradient series of acetone solutions and was then implanted in epoxy resin, sliced, stained with 2% uranium acetate, and fixed with lead citrate. Autophagosomes, autolysosomes, and phagocytic vesicles were observed under an electron microscope.

2.10. Monodansylcadaverine (MDC) staining

MOLM-13 cells were treated separately with 10 μM XN, 10 μM SPHINX31, or 500 nM gilteritinib for 12 h. The cells in the logarithmic growth phase were centrifuged (300×*g* for 3 min), and the cells were collected. The cells were washed, resuspended, and counted, and the cell concentration was adjusted to 1×10^6 cells/mL. A 900-μL cell suspension was mixed with 100 μL of MDC stain and incubated for 30 min at ambient conditions in the dark. The cells were washed and resuspended, after which 100 μL of the cell suspension was added to the slides. After the cover was placed under a fluorescence microscope (excitation filter wavelength of 355 nm, blocking filter wavelength of 512 nm), the cells were observed, counted and imaged.

2.11. In vitro Transwell invasion assay

MOLM-13 cells in the logarithmic growth phase were treated with 10 μM XN, 10 μM SPHINX31, or 500 nM gilteritinib for 24 h, with a blank control group included. The treated cells in the logarithmic phase of growth were starved and cultured for 4 h. The front side of the bottom of the chamber was coated with Matrigel (diluted 1:8), and 0.1 g/L FN was used to coat the reverse side after coagulation. The upper chamber was seeded with 200 μL of a 4×10^6 cell mixture. The bottom chamber was subsequently seeded with 600 μL of the chemotactic agent. Following a 24-h incubation period, the chamber was removed, and the cells on the upper surface were gently removed. After fixation, staining, and cleaning, the visual field was observed under a 400× inverted microscope, and the cells were imaged and counted.

2.12. Establishment of drug-resistant cell lines

The drug-resistant cell line was constructed via low-concentration induction. Gilteritinib-resistant MOLM-13 cells were generated by gradually increasing the drug concentration during the logarithmic growth phase, resulting in successful generation of the MOLM-13-R cell line. The cells were treated with an initial concentration of 20 nM, which is below the IC_{50}, for 24 h. The medium was then replaced with normal culture medium, and the cells were cultured until they reached over 80% confluence. The establishment of acquired drug-resistant cells took approximately 6 months. The drug resistance index is expressed as the resistance index (RI), and an RI greater than 5 indicates that the drug-resistant cell line was successfully generated. After successful establishment, the cells were cultured in drug-free medium for 2–3 weeks, after which the experiment was carried out. The RI was calculated as follows: resistive cell IC_{50}/parental cell IC_{50}.

2.13. Combination indices

Chou and Talalay's median effect method was used to determine the drug efficacy and the shape of the dose–effect curve. CompuSyn software was used to calculate the combination index, and a CI map was generated to evaluate the synergistic effect. A CI value greater than 1.0 indicated an antagonistic effect (the symbol represents the combined data point).

2.14. Subcutaneous tumor-bearing model

The animal experiments described in this study strictly adhered to the ARRIVE guidelines and the AVMA euthanasia guidelines of 2020 and were approved by the Experimental Animal Management and Ethics Committee of Chengdu University of Traditional Chinese Medicine (Approval No: 2022-86). Severe combined immunodeficiency (SCID) mice (male, 6 weeks old, 20–25 g) were purchased from Beijing Huafukang Biotechnology Co., Ltd. (China). The mice were housed in a barrier SPF environment, maintained at a constant temperature with a 12-h light/dark cycle, and had access to standard mouse feed and water. Human tumor cells were collected, counted, and diluted, after which 2×10^6 MOLM-13 cells were injected into the right flank of the NOD-SCID mice. The drug was dissolved in carrier buffer (5% DMSO, 40% PEG400, and 55% 50 mM 2-hydroxypropyl-β-cyclodextrin). The tumor volume was determined via the following formula: tumor volume (mm^3) = (length × $width^2$)/2. After the tumor volume reached 100 mm^3, 24 tumor-bearing mice were randomly divided into 4 groups: two XN treatment groups (40 mg/kg and 80 mg/kg), one gilteritinib group (10 mg/kg), and one control group. Each group received daily intravenous injections of the corresponding treatment in equal volumes, and the control group was given the same volume of the vehicle treatment. Changes in tumor volume were recorded once every two days. After 10 days, the mice were euthanized with pentobarbital sodium (30 mg/kg), the organs were harvested, and the tumors were removed and fixed with 4% paraformaldehyde.

2.15. HE and immunofluorescence staining

Paraffin sections were dewaxed, rehydrated, stained with hematoxylin for 5 min, stained with eosin solution for 3 min, and then subjected to gradient alcohol dehydration, xylene removal, and neutral resin sealing. Then, the paraffin sections of the tumor tissues were incubated at 60 °C, followed by xylene dewaxing and rehydration with an ethanol gradient. The cells were blocked with 0.5% Triton X-100 after antigen retrieval and 3% H_2O_2 treatment. The sections were incubated with primary antibodies overnight at 4 °C and then with secondary antibodies for 1 h the next day. After the addition of the DAPI anti-fluorescence quenching sealing solution, images were acquired via a fluorescence microscope.

2.16. Statistical analysis

The data are presented as the mean ± standard deviation (SD). An unpaired Student's t test was used for comparisons between two groups. One-way analysis of variance (ANOVA) was used for comparisons of three or more groups. Differences were considered statistically significant at $p < 0.05$.

3. Results

3.1. Initial detection of xanthohumol bioactivity and analysis of its pharmacological mechanisms against AML via network pharmacology

As illustrated in Fig. 1A, XN is a prenylated flavonoid, and its molecular structure and properties are described. To verify whether XN can affect AML, we first assessed its impact on AML cell proliferation via MTT colorimetry. The cells were treated with XN (60, 30, 15, 7.5, 3.75, or 1.88 μM) for 72 h, with a control group included. The following formula was used to calculate cell proliferation: Proliferation rate = experimental OD/control OD. The results showed that XN notably inhibited the growth of the MOLM-13 and MV4-11 cell lines in a dose-dependent manner. These differences were statistically significant. The respective IC_{50} values were 3.29 ± 1.33 μM and 8.85 ± 2.02 μM (Fig. 1B). Next, via network pharmacology, xanthohumol was analyzed to construct a drug–target network, mining targets and mechanisms for treating AML. A total of 126 XN drug-related targets and 1346 AML-related targets were identified, and 48 overlapping targets are displayed (Fig. 1C). The shared targets were imported into Cytoscape for the construction and visualization of the drug disease shared target network, which comprises 72 nodes and 141 edges (Fig. 1D). The network revealed that XN had significant cluster nodes related to cytokines, cancer pathways, transcriptional regulation, inflammation, and cell adhesion. We summarized recent reports on the anticancer effects of XN and compared them with our bioinformatics analysis. The results

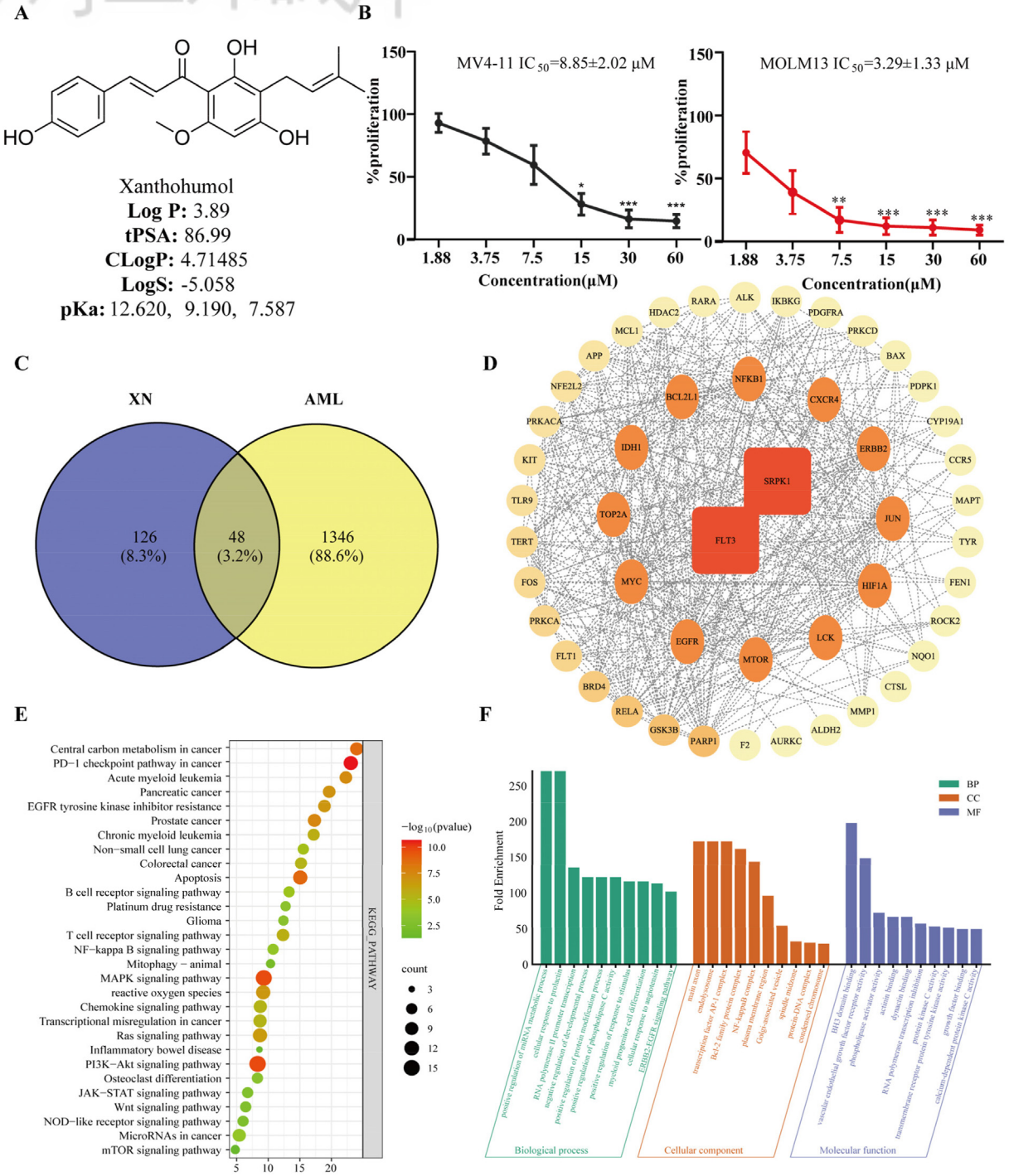

*Fig. 1. The mechanism of XN in the treatment of acute myeloid leukemia was analyzed by network pharmacology and the anti-proliferative effect of XN on AML cell types was detected. (A) The chemical structure and molecular properties of XN. (B) AML cell lines were treated with or without XN (60, 30, 15, 7.5, 3.25, 1.625 μM) for 72 h, and the proliferation rate was measured by MTT assay and IC_{50} was calculated. MOLM-13 (right); MV4-11 (left); Normalized data are expressed as the mean ± standard deviation, analysis of variance (ANOVA) test, n = 5, and p values were *p < 0.05, **p < 0.01, and ***p < 0.001 vs. the respective control. (C) The Venny 2.1.0 platform was used to construct a Venn diagram of 48 overlapping signals. (D) The Cytoscape 3.10.0 platform was used to construct an interaction network of the target pathway proteins. The red squares represent the target proteins, and the orange-yellow circles represent the cross targets according to betweenness centrality. (E) KEGG pathway enrichment analysis was performed on the bioinformatics platform. The bubble diagram shows the gene enrichment rate and pathway name; the number of genes is indicated by bubble size, and different p values are indicated by color. (F) A bioinformatics platform used to create a cross-network GO functional analysis histogram. Cyan represents BP, yellow represents CC, and blue represents MF.*

indicate that XN targets key cancer pathways, such as the PI3K-Akt and MAPK pathways. This finding aligns with that of Liu et al. [10], who predicted XN inhibits the AKT1/2 binding site in esophageal squamous cell carcinoma. Sławińska-Brych et al. [11] also found XN's anti-myeloma activity is MAPK-dependent. The differential clusters included the autophagy pathway, the apoptosis pathway, and the regulation of DNA-binding transcription factor activity (Fig. 1D and E). These results are consistent with the reports by Zhao et al. [12] and Huangfu et al. [13] that XN induces apoptosis in human liver cancer cells and alleviates impaired autophagy in pancreatitis. In addition, XN acts on cellular components (CCs), such as the nucleus, nucleoplasm, plasma membrane, mitochondria, and Bcl-2 family protein complexes. Furthermore, the enrichment of biological process (BP) terms revealed that XN is involved in the positive regulation of the angiotensin response, protein autophosphorylation, cell proliferation, kinase activity, and promoter transcription. Sun et al. [14] reported that Bax/Bcl-2 signaling improves memory in APP/PS1 mice, supporting XN's impact on Bcl-2 family proteins. The antiproliferative effect of XN aligns with that of Siahmazgi et al. [15]. Finally, the molecular function (MF) category revealed that XN is involved mainly in serine/threonine/tyrosine kinase activity, protein homodimerization activity, and ATP and chromatin binding (Fig. 1F). Lee et al. [16] also reported that XN induces NRF2 nuclear translocation and activates ARE transcription, regulating brain inflammation. These findings suggest XN has anticancer mechanisms, including regulating transcription factors and kinases that are vital for cancer cell signaling and proliferation. Our bioinformatics analysis confirms XN's known anticancer properties and offers new insights into its molecular mechanisms and target pathways in AML.

3.2. XN and SRPK1 inhibitors selectively inhibit AML proliferation

The ability of XN to target multiple factors led us to assess the selective effect of XN on other tumor cells. The results revealed stronger antitumor effects on AML cells than on other tumor cells. The SPHINX31 inhibitor had a significant inhibitory effect on AML cell lines (MOLM13 and MV4-11) but had no significant inhibitory effect on other tumor cell lines. These findings suggest that XN and its inhibitors have good selectivity for AML cell lines (Table 1).

Specifically, we treated cells with XN (60, 30, 15, 7.5, 3.75, or 1.88 μM) and SPHINX31 (40, 20, 10, 5, 2.5, or 1.25 μM) for 72 h. As shown in Table 1, the data report the selectivity index (SI) and confidence intervals (CIs) of XN for different cell lines. An SI greater than 6 indicates strong selectivity for cancer cells; $3 < SI < 6$ indicates moderate selectivity; $1 < SI < 3$ indicates slight selectivity; and an SI less than 1 indicates nonselectivity [17]. XN showed the strongest selectivity for AML cell lines, with SI values of 19.06 (MOLM-13) and 7.62 (MV4-11), both of which exceeded 6. In other cancer cells, XN exhibited moderate to low selectivity. These findings suggest that XN has high selectivity and potential for AML treatment but needs further

Table 1. The selectivity of XN/SPHINX31 to different types of cell lines.

Cell Types	Cell Lines	IC_{50}[a] (μM)		SI[b]	95%CI[c]	T value	P value
		Xanthomal	SPHINX31				
Acute myeloid leukemia	MOLM-13	3.25 ± 1.39	6.82 ± 1.94	19.06	(52.08–65.69)	24.02	$p < 0.001$
Acute myeloid leukemia	MV4-11	8.15 ± 1.32	8.84 ± 2.34	7.62	(45.24–59.95)	19.86	$p < 0.001$
Breast cancer	MDA-MB-453	18.85 ± 1.35	>40	3.49	(36.50–50.07)	17.71	$p < 0.001$
Bladder cancer	RT4	23.55 ± 13.56	>40	3.23	(15.92–61.25)	4.73	$p < 0.01$
Colon cancer	HCT116	13.52 ± 2.70	>40	4.49	(40.87–56.36)	17.42	$p < 0.001$
Colon cancer	CT26	23.56 ± 1.23	>40	2.73	(31.85–45.30)	15.92	$p < 0.001$
Cervical cancer	HELA	30.28 ± 2.07	>40	1.86	(24.62–39.09)	12.22	$p < 0.001$
Hepatobiliary cancer	HEPA1-6	16.26 ± 0.48	>40	3.87	(36.10–55.65)	19.67	$p < 0.01$
Lung cancer	NCI-H1299	11.5 ± 1.13	>40	5.70	(44.30–57.67)	21.18	$p < 0.001$
Lung cancer	A549	35.63 ± 15.13	>40	1.78	(−8.14-61.16)	2.93	$p > 0.05$
Ovary cancer	A2780	19.63 ± 7.58	>40	4.45	(28.75–56.25)	8.58	$p < 0.01$
Ovary cancer	SK-OV-3	10.12 ± 4.33	>40	4.41	(42.55–61.48)	15.26	$p < 0.001$
Pancreatic cancer	ASPC-1	31.08 ± 6.81	>40	1.57	(18.38–43.73)	6.80	$p < 0.01$
Fibroblast cell	MRC-5	62.13 ± 4.01	>40	NA[d]	NA[d]	NA[d]	NA[d]

[a] IC_{50} = Drug dosage needed for 50% inhibition of cancer cell proliferation.
[b] Tabulated values are the means ± SDs, n = 3. SI: selectivity index.
[c] 95% CI: 95% confidence interval.
[d] NA: Not applicable. The drug was ineffective for the cell lines within the test concentration range, with IC_{50} values > maximum concentration.

optimization for other cancer types. The data are presented as the means ± SDs. Differences between groups were analyzed via Student's t test from three independent experiments, with $p < 0.05$ indicating significance. The selectivity index (SI) was calculated via the following formula: SI = IC_{50} of noncancerous cells/IC_{50} of cancer cells.

3.3. In vitro kinase assay and molecular docking of FLT3/SRPK1

Recently, researchers have employed molecular docking and virtual screening techniques to identify selective FLT3 inhibitors [18,19]. They have also conducted an analysis of the structure of the SRPK/SRPIN340 complex [20], indicating that the inhibition of FLT3 and SRPK might constitute a potential therapeutic strategy. On this basis, we used the same methods to successfully dock XN into the ATP binding pocket of the FLT3 protein (PDB ID: 1RJB) and SRPK1 protein (PDB ID: 7DD1), forming stable SRPK/XN and FLT3/XN complexes (Fig. 2A–D). The crystal structures of FLT3 and SRPK1 were obtained from the Protein Data Bank (PDB, http://www.pdb.org). All the ligands were drawn via ChemDraw22.2.0, and 3D structures were established and minimized via the MM2 force field in Chem3Dpro for docking. Specifically, XN formed hydrogen bonds (HBs) with the active site amino acid residues Glu573 and Asp829 of FLT3 (Fig. 2A), whereas gilteritinib formed hydrogen bonds with the Ala896 and Glu862 residues of FLT3 (Fig. 2B). Additionally, XN formed hydrogen bonds with the Tyr616, Ala545, and Ser179 residues of SRPK1 (Fig. 2C), whereas SPHINX31 formed hydrogen bonds with the Ile566, Glu552, and Lys604 residues of SRPK1 (Fig. 2D). Docking was performed with AutoDockTools-1.5.6 and visualized in 3D with PyMOL, revealing the number and length of hydrogen bonds and the connected amino acid residues. The hydrogen bonds are illustrated as yellow dashed lines. The binding energies of XN to FLT3 and SRPK1 were −15.69 and −25.61 kJ/mol, respectively. The binding energies of gilteritinib and SPHINX31 were −33.30 and −26.57 kJ/mol, respectively. XN has a high score for docking with the receptor, a strong binding energy, and a stable conformation.

According to the results of homogeneous time-resolved fluorescence (HTRF) detection, XN effectively inhibited the *in vitro* and cellular kinase activities of FLT3 and SRPK1 at various concentrations (10, 3.33, 1.11, 0.37, 0.12 and 0.04 μM) (Fig. 2E and F). The HTRF results demonstrated that XN acts directly on the FLT3 and SRPK1 protein kinases.

3.4. XN inhibits the FLT3/SRPK1 signaling pathway in AML cells

Using Western blotting, we investigated the effects of XN on the levels of kinase-mediated phosphorylation of FLT3 and SRPK1 signaling pathway components. The Western blotting results revealed that XN effectively inhibited the expression levels of p-FLT3 and p-SRPK1 in a concentration-dependent manner (Fig. 2G and H). We observed that FLT3 and SRPK1 activity was decreased in XN-treated MOLM-13 cells. SPHINX31 can significantly reduce FLT3 phosphorylation levels, while treatment with the selective FLT3 inhibitor gilteritinib also inhibits SRPK1. In addition, the drug disease composite target network intersection supports a potential link between FLT3 and SRPK1 in cell signal transduction. This series of evidence points to potential interactions between FLT3 and SRPK1 that affect cellular functions. Furthermore, we investigated the dynamic changes in signaling pathways by monitoring the protein expression levels of regulatory factors at different time points (0, 4, and 8 h) (Fig. 2I and J). Phosphorylated FLT3 and SRPK1 proteins degraded gradually between 4 and 8 h posttreatment and notably decreased at 24 h. While pERK protein levels did not significantly change at 0, 4, and 8 h, they notably decreased at 24 h. Phosphorylated ERK1/2 levels also decreased over time, indicating that XN inhibits sustained activation signaling mediated by FLT3.

3.5. XN blocks the cell cycle and induces apoptosis in MOLM-13 cells

Through flow cytometry, we observed that XN significantly increased the proportions of early and late apoptotic MOLM-13 cells in a dose-responsive manner (Fig. 3A and C). Hoechst 33258 staining revealed that XN induced apoptosis in MOLM-13 cells, and typical characteristics of apoptosis, namely, bright blue fluorescence, cell shrinkage, cell rounding, chromatin condensation, and deep staining, were observed (Fig. 3E). XN induced cell cycle arrest at the G0/G1 phase and reduced the proportion of MOLM-13 cells in the S and G2/M phases. Furthermore, SPHINX31 had a more pronounced inhibitory effect (Fig. 3B and D).

To elucidate the mechanism through which SRPK1 activation may influence tumor proliferation in AML patients, we assessed the differential expression of downstream effector proteins in SRPK1-induced tumors. Specifically, we investigated the expression of BRD4-induced G1 cell cycle arrest or CMYC, which are known downstream

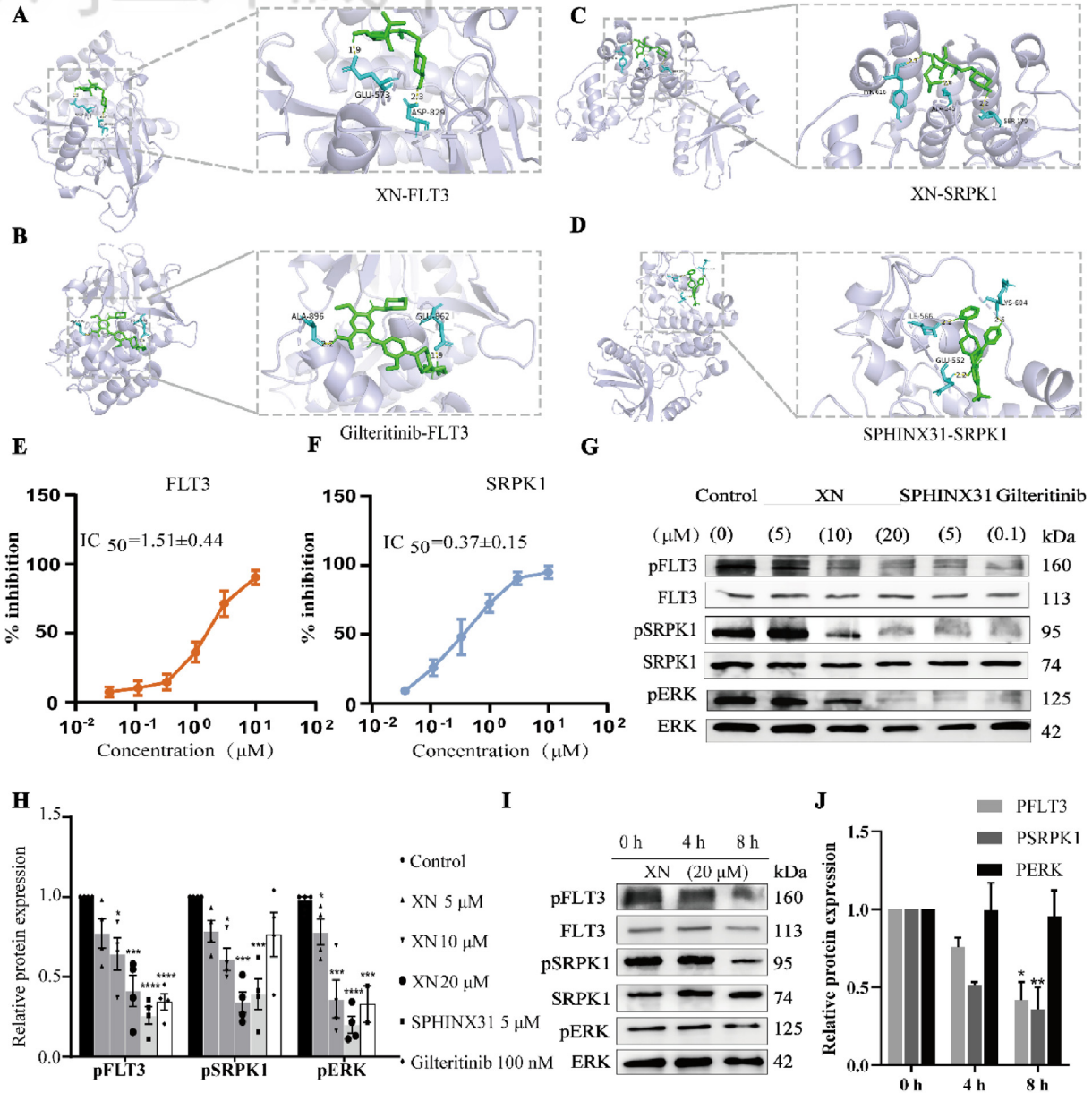

*Fig. 2. Inhibitory effects of XN on kinase activity and molecular docking verification. (A–D) Three-dimensional diagrams of molecular docking interaction between FLT3/XN, SRPK1/XN, FLT3/Gilteritinib and SRPK1/SPHINX31 complexes. Ligand molecules are green, amino acid residues are highlighted in blue, and hydrogen bonds are represented by yellow dotted lines. The images were created by AutoDock. (E, F) HTRF was employed to determine the inhibitory effect of XN on the FLT3 and SRPK1 kinases. (G, H) MOLM-13 cells were treated with XN (5 μM, 10 μM, and 20 μM), Gilteritinib (100 nM), or SPHINX31 (5 μM) for 24 h. The expression levels of FLT3, pFLT3, SRPK1, pSRPK1,ERK and pERK, proteins were analyzed by Western blot. The proteins were quantified using ImageJ software. Ratios of gray values of target phosphorylated proteins to the corresponding total proteins were calculated. pSRPK1, pFLT3, and pERK were normalized to their respective total proteins and presented as fold-change relative to DMSO. (I, J) Western blot analysis and quantification of key signaling proteins FLT3, pFLT3, SRPK1, pSRPK1, ERK, and pERK at different time points (0, 4, and 8 h) after XN treatment. (n = 3 per time point). The above data were analyzed by one-way analysis of variance (ANOVA). Normalized data are presented as the means ± SDs, with p values of *p < 0.05, **p < 0.01, and ***p < 0.001 vs. the respective control.*

targets of SRPK1 [21,22]. Additionally, the BET family protein BRD4 plays a crucial role in AML by modulating NF-kB signaling and inhibiting AML cell proliferation through interference with the Bcl2/Bax apoptotic pathways [23–27]. Our results revealed that XN treatment in MOLM-13 cells decreased the phosphorylation of SRPK1-mediated proteins such as BRD4 and NF-κB, and induced alterations in the levels of apoptosis-associated proteins such as BAX and BCL2 (Fig. 3F–H).

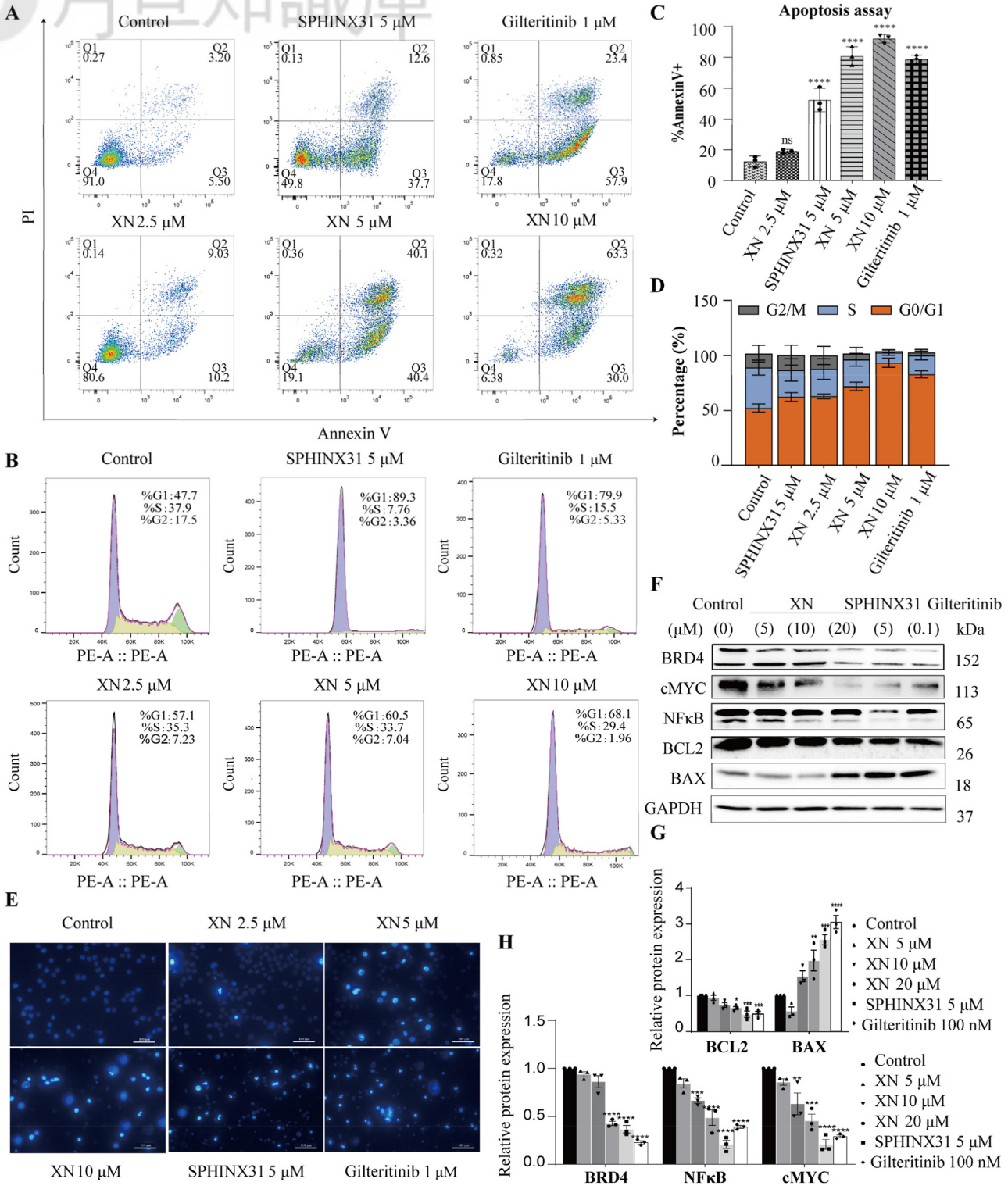

*Fig. 3. XN blocks MOLM-13 cell cycle progression and induces apoptosis. MOLM-13 cells were treated with or without XN (2.5, 5, 10 μM), Gilteritinib (1 μM), SPHINX31 (5 μM) for 48 h. After Annexin V-FITC/PI staining, at least 10,000 cells were collected for flow cytometry analysis. (A) The proportion of cells undergoing apoptosis that were both Annexin V-positive (indicating early apoptosis) and PI-positive (indicating late apoptosis). FlowJo (version 10.1r5) was used for cell cycle and apoptosis analysis. (B) Flow cytometry was used to evaluate the cell cycle distribution. (C–D) A representative bar chart of the cell cycle/apoptosis distribution is shown. The data are presented as the means ± standard deviations, with asterisks denoting statistical significance. (E) Staining with Hoechst 33258 (10 μg/mL) determined the presence of apoptotic cells. Representative images of cells treated with different drug concentrations of each treatment were observed under an inverted fluorescence microscope. (F–H) MOLM-13 cells were exposed to varying concentrations of XN, Gilteritinib, or SPHINX31 for 24 h, followed by protein expression analysis for cell cycle and apoptosis-related markers. All the above data were expressed as the mean ± standard deviation, analysis of variance (ANOVA) test, n = 3, and p values were *p < 0.05, **p < 0.01, and ***p < 0.001 vs. the respective control.*

3.6. XN enhances AML autophagosome formation and impairs invasion

After treatment with XN, transmission electron microscopy (TEM) revealed that the number of autophagic vacuoles in MOLM-13 cells increased, and morphological changes occurred at different stages of autophagosome formation (Fig. 4A). The MDC method was used to detect probe-labeled autophagosomes, and the results once again demonstrated that XN treatment promoted autophagy (Fig. 4B and D). Transwell invasion assays

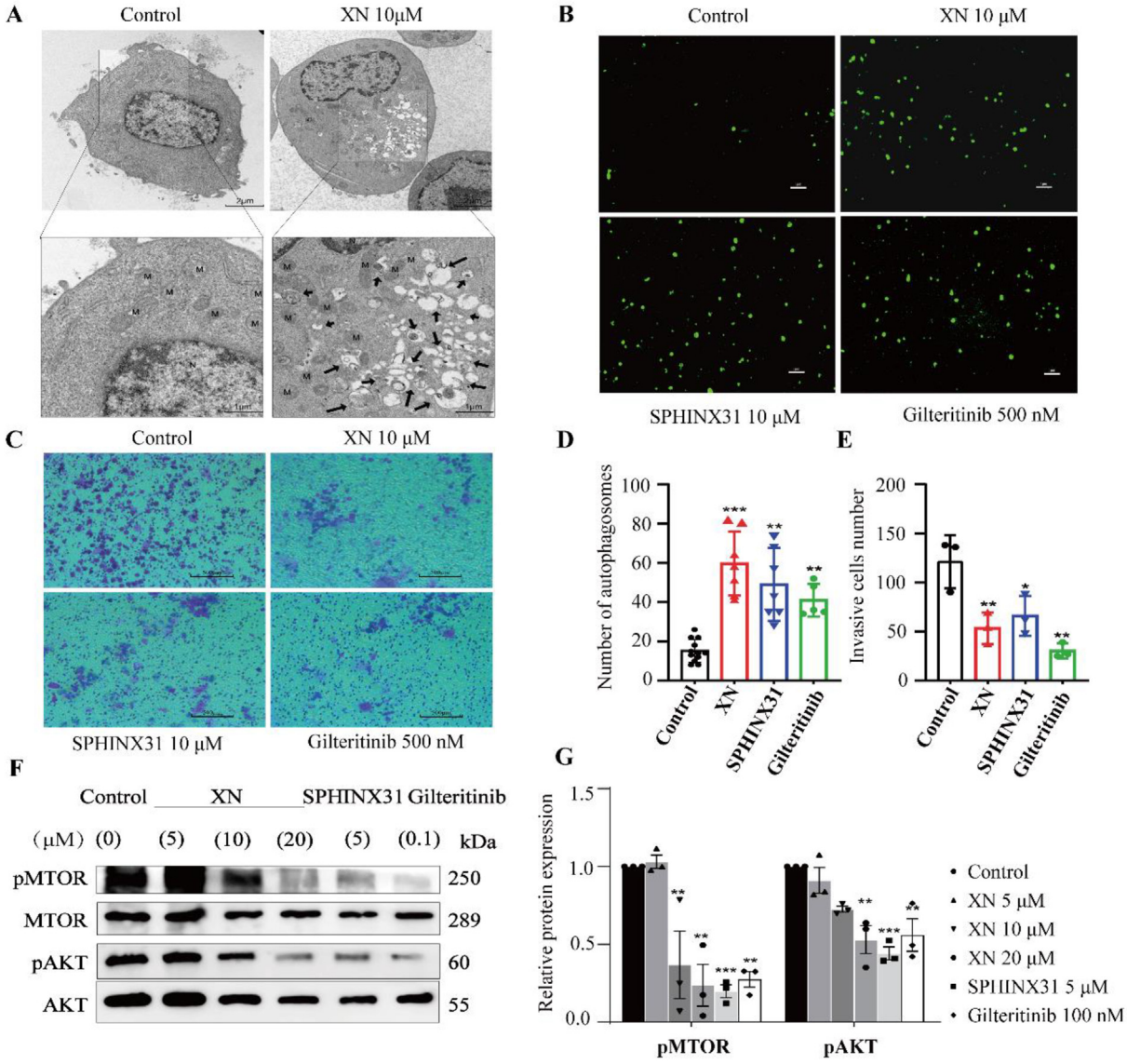

*Fig. 4. Effects of XN on MOLM-13 cell autophagy and invasion. MOLM-13 cells were treated with XN (10 μM), SPHINX31 (10 μM), Gilteritinib (500 nM), and DMSO treatment was used as a control group. (A) The number of autophagic vacuoles in MOLM-13 cells that were treated with or without XN (10 μM) for 16 h was observed by transmission electron microscopy. Autophagosomes are indicated by black arrows. 'N' represents the nucleus, and 'M' represents mitochondria. (Scale: 2 μm; raw magnification **2000**×, upper panels). (Scale: 1 μm; original magnification **5000**×, lower panels). (B, D) An MDC staining kit was used to determine the formation and quantification of autophagosomes in MOLM-13 cells labeled with MDC autophagosome markers. The representative autophagy images and quantitative results of MOLM-13 cells were treated with MDC. Scale: 1 μm. (C, E) A Transwell assay was used to assess the impact of xanthohumol and inhibitors on the invasion ability of MOLM-13 cells, with DMSO-treated cells serving as the control group for imaging and quantitative analysis. An inverted optical microscope was used to capture images of cells on the porous membrane in three randomly selected microscope fields per well, and the ImageJsoftware was used for counting. (F–G) MOLM-13 cells were exposed to varying concentrations including 5, 10, 20 μM XN, 5 μM SPHINX31, or 100 nM Gilteritinib for 24 h, with a control set. ImageJ analysis software quantified the expression levels of autophagy and invasion-related proteins (pAKT/AKT, pMTOR/MTOR). All data are presented as means ± SDs, $n = 3$, with p values denoted as $^{*}p < 0.05$, $^{**}p < 0.01$, and $^{***}p < 0.001$ vs. the respective control.*

revealed that, compared with the control group (121 ± 27 cells), the experimental group treated with XN presented significantly reduced cell invasion (53 ± 16 cells) (*$p < 0.05$) (Fig. 4C and E). Our results showed that XN regulates the ability of AML cells to form autophagosomes and blocks cell invasion.

FLT3 activates downstream effectors, with ERK inhibition controlling invasion, while the activation of phospho-AKT1 and phospho-MTOR plays essential roles in development by modulating autophagy [28–31]. XN reduces invasion potential, indicating that the ERK pathway is activated during AML invasion. This finding is in line with the previous observation that treatment with XN led to a significant reduction in the relative phosphorylation level of ERK in MOLM-13 cells. Furthermore, XN treatment increased autophagy in MOLM-13 cells, which was associated with AKT/mTOR pathway inhibition. XN blocks FLT3-dependent pathways, including the AKT/mTOR and MAPK/ERK pathways, as shown in Fig. 4. XN significantly regulates FLT3 and its downstream effectors, impacting AML autophagosomes and invasion (Fig. 4F and G).

3.7. XN and SPHINX31 are sensitive to gilteritinib-resistant MOLM-13 cells, which synergize with an FLT3 inhibitor

The results revealed that the IC_{50} values in MOLM-13 cells before and after the establishment of gilteritinib resistance were 0.08 ± 0.06 μM and 1.25 ± 0.68 μM, respectively. The resistance index (RI) was calculated as 15.125, confirming the successful establishment of the gilteritinib-resistant cell line, named MOLM-13-R (Fig. 5A). Various concentrations of XN (left) and SPHINX31 (right) maintained sensitivity in both MOLM-13 parental and drug-resistant cell lines (Fig. 5B). The IC_{50} values of gilteritinib, XN, and SPHINX31 in the parental AML cell lines were 42.4 nM, 1.33 μM, and 21.97 μM, respectively. Drug-resistant cells were sensitive to XN and SPHINX31, with IC_{50} values of 1.44 μM and 10.04 μM, respectively; however, MOLM-13-R cells were resistant to gilteritinib, and the difference was statistically significant (IC_{50} > 100 Nm, Fig. 5C and D). We used a series of diluents with fixed molar ratios (1:10, 1:20, and 1:30) to determine the combination index (CI) values (Fig. 5E and F). The CI value of treatment (1:30) with both XN and gilteritinib was 0.243, whereas treatment with both gilteritinib and SPHINX31 (1:0.5) resulted in a CI value of 0.543 in MOLM-13 cells. The CI values in the MOLM-13-R cells were 0.224 and 0.716, respectively. These results demonstrate that XN and SPHINX31 maintain sensitivity in both gilteritinib-resistant cells and nonresistant MOLM-13 cells, with the combination of gilteritinib exhibiting synergy. These findings suggest that the combination of XN with gilteritinib may effectively treat both primary and recurrent AML.

3.8. XN inhibits AML tumor growth in vivo

XN significantly decreased the growth of AML tumors and promoted their death *in vivo* in a dose-dependent manner (Fig. 6A). In contrast to that in the control group (1.17 ± 0.14 cm^3), the tumor volume in the XN group (0.74 ± 0.18 cm^3, 0.36 ± 0.17 cm^3) and gilteritinib group (0.09 ± 0.08 cm^3) decreased by 36.7%, and 69.2%, respectively, in a dose-dependent manner. The average body weight of the control group was 27.1 ± 2.17 g, and the average body weights of the treatment groups were 26.0 ± 1.47 g, 25.6 ± 2.03 g, and 25.7 ± 1.35 g, respectively (Fig. 6B). No significant weight loss was observed in the mice. In xenograft tumor sections, XN significantly decreased the quantity of Ki-67-positive tumor cells. Concurrently, the TUNEL data indicated that XN effectively induced apoptosis in tumor cells (Fig. 6C–E). Upon autopsy, no evidence of edema or abnormal organ size was noted in the mice. Furthermore, hematoxylin and eosin staining revealed that XN did not induce notable cytotoxicity in mouse organs (Fig. 6F). We used Western blotting to analyze key regulatory factors in excised tumor tissues. The results showed that XN inhibited FLT3 and SRPK1 phosphorylation in a dose-dependent manner. These findings suggest that XN affects tumor cell growth and proliferation by regulating the activation of FLT3 and SRPK1 (Fig. 6G). The above results indicate that XN effectively inhibits tumor growth and promotes tumor cell apoptosis *in vivo*, further supporting the potential of XN as a candidate antitumor drug.

4. Discussion

Our study reveals for the first time that XN inhibits the proliferation of AML cells and exerts multiple anti-AML effects via its ability to inhibit the FLT3/SRPK1 axis (Fig. 1); these results reveal new possibilities for the development of more effective drugs for the treatment of AML. By downregulating phosphorylated FLT3 and SRPK1 levels, XN regulates the interaction of downstream signaling pathways, thereby effectively inhibiting the proliferation and growth of AML. The structure of XN allows it to form specific hydrogen bonds with key amino acid

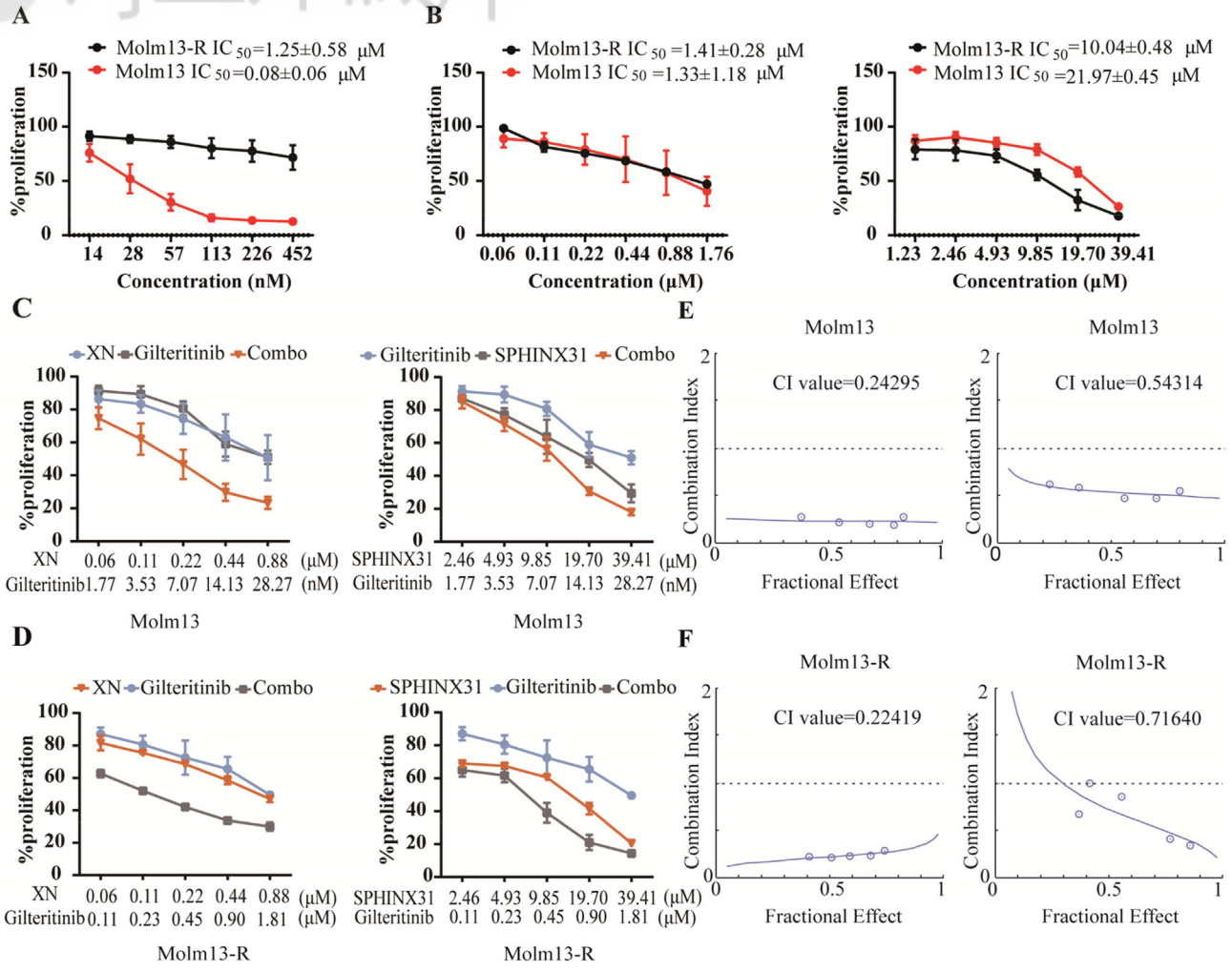

Fig. 5. XN inhibits the proliferation of the parental and drug-resistant MOLM-13 cell lines and exerts synergistic effects with Gilteritinib. (A) An MTT assay was used to detect the proliferation changes of MOLM-13 cells before and after resistance to Gilteritinib, and IC_{50} values were compared. (B) Under the same concentration gradient, the proliferation of the MOLM-13 parental cell line and drug-resistant cell line (MOLM-13-R) was detected with XN treatment (left graph) and SPHINX31 treatment (right graph), and IC_{50} was calculated. (C, D) Dose-response curves of MOLM-13 and MOLM-13-R cells treated with Gilteritinib, XN (left), or SPHINX31 (right) alone, and in combination at a constant ratio were generated. (C: The cells used were MOLM-13; D: The cells used were MOLM-13-R). (E, F) Under constant ratio conditions, FA-CI curves simulated using CompuSyn software were analyzed to assess the synergy of the same combination treatments (CI) values were determined. Gilteritinib with XN (left) and Gilteritinib with SPHINX31 (right); (E: The cells used were MOLM-13; F: The cells used were MOLM-13-R).

residues in the active pockets of FLT3 and SRPK1, thereby inhibiting kinase activity (Fig. 2). This unique dual specificity of XN allows it to simultaneously exert different anti-AML effects. For example, XN promotes AML cell apoptosis and induces G0/G1 phase arrest in a dose-dependent manner; additionally, XN strongly inhibits AML cell proliferation (Fig. 3), decreases invasion and induces autophagy to prevent the progression and spread of AML (Fig. 4). Furthermore, parental or drug-resistant MOLM-13 cells were sensitive to XN, which exerts synergistic effects with FLT3 TKIs against AML (Fig. 5). XN treatment effectively inhibited tumor growth in mice, but no adverse toxic events were observed, indicating the safety of XN treatment (Fig. 6). This study revealed that XN has the potential to prevent and treat AML.

Recent studies on XN and its derivatives in leukemia have focused mainly on chronic myeloid leukemia [32–35], acute and chronic lymphoid leukemia [36–38], and single other types of leukemia [39,40]. However, little is known about the role of XN in acute myeloid leukemia. Studies have shown that XN can play a regulatory role in cell proliferation, transformation, autophagy, and antiapoptotic effects through various molecular pathways such as the NF-κB, MAPK, ROS, and AMPK pathways, or affect chemotherapy resistance through endoplasmic reticulum stress [41–44]. Despite these findings, comprehensive research on specific

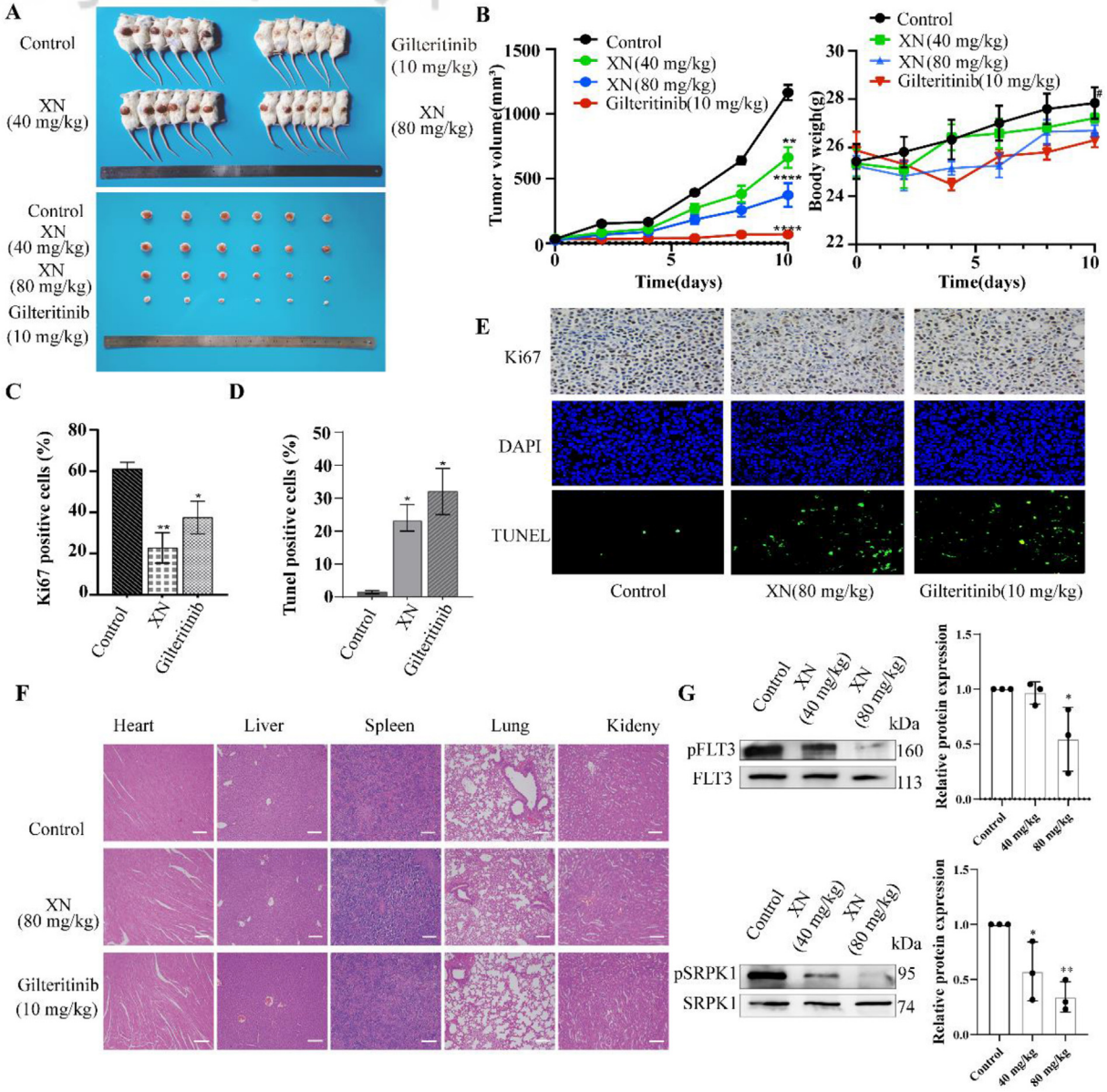

Fig. 6. The anti-tumor effect of XN in vivo in the subcutaneous xenograft model of NOD-SCID mice. (A) Images of subcutaneous tumors in mice given or not given XN (40 mg/kg, 80 mg/kg), Gilteritinib (10 mg/kg), and representative images of excised xenograft tumors. (B) The changes in the body weight of mice and the tumor volume growth curve after receiving XN treatment (6 mice per group); the weights of the mice and the volumes of the tumors were documented every other day. (C–E) Representative image and quantitative analysis of Ki-67 expression and TUNEL staining in tumor tissue by XN. (F) Representative image of H&E-stained mouse heart, liver, spleen, lung, and kidney tissue sections; scale: 100 μm. (G) Western blot images showing the expression levels of pFLT3 and total FLT3, pSRPK1 and total SRPK1 proteins in tumor tissue extracts from mice. The relative phosphorylation levels were normalized to the total protein expression using ImageJ software and presented as fold changes compared to the control. All data are expressed as the mean ± standard deviation, with statistical significance between groups determined by ANOVA, $n = 3$, with p values of $^{*}p < 0.05$, $^{**}p < 0.01$, and $^{*}p < 0.001$.

mechanisms and interactions is lacking. Most studies are limited to cell models and lack verification in animal models [45–48]. The aim of our study was to address this gap by focusing on AML, using advanced technologies and immunodeficiency animal models to illustrate the significant therapeutic effects and unique mechanisms of XN, and exploring its synergistic potential with conventional chemotherapy.

The results of the present study revealed that XN exerts a significant and selective inhibitory effect on AML cells. In addition to its anticancer effects, the diverse pharmacological effects of XN have broad application prospects. XN can be used as an

antioxidant to prevent several chronic diseases caused by oxidative stress [49,50], inhibit proinflammatory cytokine production, and reduce inflammation [51]; moreover, its antimicrobial properties allow it to be used for food preservation [52,53]. However, the benefits of XN are accompanied by potential drawbacks. For example, although XN has antioxidant capacity, the structure of polyphenols is extremely unstable, and they can easily decompose when exposed to light [54]. Moreover, its low solubility and enterohepatic circulation lead to poor biological absorption, rapid metabolism, and excretion, limiting its bioavailability [55,56]. Therefore, 2-hydroxypropyl-β-cyclodextrin and intravenous injection were used in this study to improve the drug stability and bioavailability of XN. Similarly, a regular diet generally cannot provide high doses of XN, while supplements can offer relatively high concentrations of XN to support specific nutritional needs and overall health of the body.

Currently, XN still has numerous limitations in basic research and clinical application. Primarily, existing research has focused predominantly on a limited number of leukemia cell lines, and validation in diverse AML models and animal models is lacking. Furthermore, while XN has inhibitory effects on specific pathways, its potential off-target effects may impact unforeseen cellular processes, leading to adverse reactions, albeit not entirely understood. Therefore, comprehensive biological screening and analysis are imperative to ensure the specificity and safety of XN.

Moreover, the bioavailability and stability of XN are pivotal factors determining its potential for clinical application [57]. Genetically engineered microorganisms or modified chemical synthesis methods can be enhanced to improve yield and purity [58,59]. Prodrug design or modifications such as esterification can increase solubility and stability [60,61]. Additionally, nanocarrier systems such as liposomes and polymer nanoparticles can increase the stability and *in vivo* absorption efficiency [62]. Consequently, future research could explore improvements in the preparation process, modifications of the chemical structure, or changes in dosage forms to achieve wider and more efficient application of XN.

Some of our preliminary work has laid the groundwork for its clinical translation. We have demonstrated the efficacy of XN in targeting FLT3 and SRPK1 in drug-resistant cells, as well as its efficacy and safety in animal models. This preliminary work will continue to progress toward clinical trials, including optimizing doses and dosing regimens, conducting toxicity and safety assessments, completing pharmacokinetic and pharmacodynamic analyses, and exploring the combined efficacy with other chemotherapeutic drugs. In the future, we plan to test XN in more complex animal models, conduct long-term safety and toxicity studies, and initiate preliminary human clinical trials to ensure the feasibility and reliability of its clinical application.

As a tumor promoter, abnormal SRPK1 regulates splicing and mRNA expression, causing a variety of diseases, such as Alzheimer's disease [63], neovascular eye disease [64], kidney disease [65], diabetes [66], arthritis [67] and atherosclerosis [68], and affecting inflammation-related transcription factors and signaling pathways [69]. Similarly, FLT3 is not only associated with AML but also involved in the pathogenesis of lung cancer, colorectal cancer, and thyroid cancer [70,71]. These findings led us to further study whether XN has dual targeting effects on diseases such as colitis, arthritis, and diabetes to optimize its clinical application.

Overall, we found that XN can be used as a potential therapeutic agent for AML and that XN functions by targeting FLT3 and SRPK1; moreover, the efficacy and safety of this agent were confirmed. XN can regulate proliferation, autophagy, invasion, and drug resistance via multiple mechanisms and compensate for the limitations of single agents. Our findings increase the likelihood of developing new treatments for AML patients and provide new evidence that supplements existing knowledge of the mechanisms involved in treating AML. In general, our study supports the use of XN in the treatment of AML and suggests that XN may also be a potential therapy for other types of tumors.

Declaration of competing interest

The authors disclose no financial conflicts.

Acknowledgments

This study was supported by the National Natural Science Foundation of China (82174193, 82374245), the Xinglin Scholar Talent Research Supporting Program of CDUTCM (QNTD2022001, QNRC2022012), and the Sichuan Province Foundation for Natural Sciences (2022JDJQ0058, 2023YFS0110). We appreciate the assistance provided by the CDUTCM State Key Laboratory in supplying the experimental equipment. Graphical abstract was created by Figdraw (http://www.figdraw.com;this material ID: UPUTO4143b).

References

[1] Daver N, Schlenk RF, Russell NH, Levis MJ. Targeting FLT3 mutations in AML: review of current knowledge and evidence. Leukemia 2019;33:299–312.

[2] Bae KH, Lai F, Chen Q, Kurisawa M. Potentiating gilteritinib efficacy using nanocomplexation with a hyaluronic acid-epigallocatechin gallate conjugate. Polymers (Basel) 2024;16.

[3] Duggan WP, O'Connell E, Prehn JHM, Burke JP. Serine-Arginine Protein Kinase 1 (SRPK1): a systematic review of its multimodal role in oncogenesis. Mol Cell Biochem 2022;477: 2451−67.

[4] Patel M, Sachidanandan M, Adnan M. Serine arginine protein kinase 1 (SRPK1): a moonlighting protein with theranostic ability in cancer prevention. Mol Biol Rep 2019;46: 1487−97.

[5] Siqueira RP, Caetano MMM, de Souza LA, Dos Passos PMS, Simaroli NB, Barros MVA, et al. Combined SRPK and AKT pharmacological inhibition is synergistic in T-cell acute lymphoblastic leukemia cells. Toxicol Vitro 2020;65:104777.

[6] Tram J, Mesnard JM, Peloponese Jr JM. Alternative RNA splicing in cancer: what about adult T-cell leukemia? Front Immunol 2022;13:959382.

[7] Sinnakannu JR, Lee KL, Cheng S, Li J, Yu M, Tan SP, et al. SRSF1 mediates cytokine-induced impaired imatinib sensitivity in chronic myeloid leukemia. Leukemia 2020;34: 1787−98.

[8] Tzelepis K, De Braekeleer E, Aspris D, Barbieri I, Vijayabaskar MS, Liu WH, et al. SRPK1 maintains acute myeloid leukemia through effects on isoform usage of epigenetic regulators including BRD4. Nat Commun 2018;9: 5378.

[9] Tzelepis K, Koike-Yusa H, De Braekeleer E, Li Y, Metzakopian E, Dovey OM, et al. A CRISPR Dropout screen identifies genetic vulnerabilities and therapeutic targets in acute myeloid leukemia. Cell Rep 2016;17:1193−205.

[10] Liu X, Song M, Wang P, Zhao R, Chen H, Zhang M, et al. Targeted therapy of the AKT kinase inhibits esophageal squamous cell carcinoma growth in vitro and in vivo. Int J Cancer 2019;145:1007−19.

[11] Slawinska-Brych A, Zdzisinska B, Czerwonka A, Mizerska-Kowalska M, Dmoszynska-Graniczka M, Stepulak A, et al. Xanthohumol exhibits anti-myeloma activity in vitro through inhibition of cell proliferation, induction of apoptosis via the ERK and JNK-dependent mechanism, and suppression of sIL-6R and VEGF production. Biochim Biophys Acta Gen Subj 2019;1863:129408.

[12] Zhao X, Jiang K, Liang B, Huang X. Anticancer effect of xanthohumol induces growth inhibition and apoptosis of human liver cancer through NF-kappaB/p53-apoptosis signaling pathway. Oncol Rep 2016;35:669−75.

[13] Huangfu Y, Yu X, Wan C, Zhu Y, Wei Z, Li F, et al. Xanthohumol alleviates oxidative stress and impaired autophagy in experimental severe acute pancreatitis through inhibition of AKT/mTOR. Front Pharmacol 2023;14:1105726.

[14] Sun XL, Zhang JB, Guo YX, Xia TS, Xu LC, Rahmand K, et al. Xanthohumol ameliorates memory impairment and reduces the deposition of beta-amyloid in APP/PS1 mice via regulating the mTOR/LC3II and Bax/Bcl-2 signalling pathways. J Pharm Pharmacol 2021;73:1230−9.

[15] Gholizadeh Siahmazgi Z, Irani S, Ghiaseddin A, Fallah P, Haghpanah V. Xanthohumol hinders invasion and cell cycle progression in cancer cells through targeting MMP2, MMP9, FAK and P53 genes in three-dimensional breast and lung cancer cells culture. Cancer Cell Int 2023;23:153.

[16] Lee IS, Lim J, Gal J, Kang JC, Kim HJ, Kang BY, et al. Anti-inflammatory activity of xanthohumol involves heme oxygenase-1 induction via NRF2-ARE signaling in microglial BV2 cells. Neurochem Int 2011;58:153−60.

[17] Csuvik O, Szemeredi N, Spengler G, Szatmari I. Synthesis of 4-hydroxyquinolines as potential cytotoxic agents. Int J Mol Sci 2022;23.

[18] Gokhale P, Chauhan APS, Arora A, Khandekar N, Nayarisseri A, Singh SK. FLT3 inhibitor design using molecular docking based virtual screening for acute myeloid leukemia. Bioinformation 2019;15:104−15.

[19] Ouassaf M, Daoui O, Alam S, Elkhattabi S, Belaidi S, Chtita S. Pharmacophore-based virtual screening, molecular docking, and molecular dynamics studies for the discovery of novel FLT3 inhibitors. J Biomol Struct Dyn 2023;41: 7712−24.

[20] Siqueira RP, Barbosa Ede A, Poleto MD, Righetto GL, Seraphim TV, Salgado RL, et al. Potential antileukemia effect and structural analyses of SRPK inhibition by N-(2-(Piperidin-1-yl)-5-(Trifluoromethyl)Phenyl)Isonicotinamide (SRPIN340). PLoS One 2015;10:e0134882.

[21] Jin N, George TL, Otterson GA, Verschraegen C, Wen H, Carbone D, et al. Advances in epigenetic therapeutics with focus on solid tumors. Clin Epigenet 2021;13:83.

[22] Wan L, Deng M, Zhang H. SR splicing factors promote cancer via multiple regulatory mechanisms. Genes (Basel) 2022;13.

[23] Yang J, Song C, Zhan X. The role of protein acetylation in carcinogenesis and targeted drug discovery. Front Endocrinol (Lausanne) 2022;13:972312.

[24] Jia Q, Chen S, Tan Y, Li Y, Tang F. Oncogenic super-enhancer formation in tumorigenesis and its molecular mechanisms. Exp Mol Med 2020;52:713−23.

[25] Moris D, Ntanasis-Stathopoulos I, Tsilimigras DI, Adam MA, Yang CF, Harpole D, et al. Insights into novel prognostic and possible predictive biomarkers of lung neuroendocrine tumors. Cancer Genomics Proteomics 2018; 15:153−63.

[26] Kubina R, Krzykawski K, Kabala-Dzik A, Wojtyczka RD, Chodurek E, Dziedzic A. Fisetin, a potent anticancer flavonol exhibiting cytotoxic activity against neoplastic malignant cells and cancerous conditions: a scoping, comprehensive review. Nutrients 2022;14.

[27] Hajialyani M, Hosein Farzaei M, Echeverria J, Nabavi SM, Uriarte E, Sobarzo-Sanchez E. Hesperidin as a neuroprotective agent: a review of animal and clinical evidence. Molecules 2019;24.

[28] Ikeda D, Chi S, Uchiyama S, Nakamura H, Guo YM, Yamauchi N, et al. Molecular classification and overcoming therapy resistance for acute myeloid leukemia with adverse genetic factors. Int J Mol Sci 2022;23.

[29] Greiner J, Gotz M, Wais V. Increasing role of targeted immunotherapies in the treatment of AML. Int J Mol Sci 2022;23.

[30] Ju X, Tang Y, Qu R, Hao S. The emerging role of circ-SHPRH in cancer. OncoTargets Ther 2021;14:4177−88.

[31] Zhang H, Chen L, Sun X, Yang Q, Wan L, Guo C. Matrine: a promising natural product with various pharmacological activities. Front Pharmacol 2020;11:588.

[32] Monteghirfo S, Tosetti F, Ambrosini C, Stigliani S, Pozzi S, Frassoni F, et al. Antileukemia effects of xanthohumol in Bcr/Abl-transformed cells involve nuclear factor-kappaB and p53 modulation. Mol Cancer Therapeut 2008;7:2692−702.

[33] Matsumoto K, Akao Y, Kobayashi E, Ito T, Ohguchi K, Tanaka T, et al. Cytotoxic benzophenone derivatives from Garcinia species display a strong apoptosis-inducing effect against human leukemia cell lines. Biol Pharm Bull 2003;26: 569−71.

[34] Harikumar KB, Kunnumakkara AB, Ahn KS, Anand P, Krishnan S, Guha S, et al. Modification of the cysteine residues in IkappaBalpha kinase and NF-kappaB (p65) by xanthohumol leads to suppression of NF-kappaB-regulated gene products and potentiation of apoptosis in leukemia cells. Blood 2009;113:2003−13.

[35] Lu X, Geng J, Zhang J, Miao J, Liu M. Xanthohumol, a prenylated flavonoid from hops, induces caspase-dependent degradation of oncoprotein BCR-ABL in K562 cells. Antioxidants (Basel) 2019;8.

[36] Benelli R, Vene R, Ciarlo M, Carlone S, Barbieri O, Ferrari N. The AKT/NF-kappaB inhibitor xanthohumol is a potent anti-lymphocytic leukemia drug overcoming chemoresistance and cell infiltration. Biochem Pharmacol 2012;83:1634−42.

[37] Chen B, Yi B, Mao R, Liu H, Wang J, Sharma A, et al. Enhanced T cell lymphoma in NOD.Stat5b transgenic mice is caused by hyperactivation of Stat5b in CD8+ thymocytes. PLoS One 2013;8:e56600.

[38] Lust S, Vanhoecke B, Janssens A, Philippe J, Bracke M, Offner F. Xanthohumol kills B-chronic lymphocytic leukemia cells by an apoptotic mechanism. Mol Nutr Food Res 2005;49: 844–50.

[39] Teisseyre A, Chmielarz M, Uryga A, Sroda-Pomianek K, Palko-Labuz A. Co-application of statin and flavonoids as an effective strategy to reduce the activity of voltage-gated potassium channels Kv1.3 and induce apoptosis in human leukemic T cell line Jurkat. Molecules 2022;27.

[40] Zolnierczyk AK, Maczka WK, Grabarczyk M, Winska K, Wozniak E, Aniol M. Isoxanthohumol–Biologically active hop flavonoid. Fitoterapia 2015;103:71–82.

[41] Lust S, Vanhoecke B, Vang M, Boelens J, H VANM, Kaileh M, et al. Xanthohumol activates the proapoptotic arm of the unfolded protein response in chronic lymphocytic leukemia. Anticancer Res 2009;29:3797–805.

[42] Wang CM, Huo X, Chen J, Liu JW, Yang TY, Mi XQ, et al. An acute lytic cell death induced by xanthohumol obstructed ROS detecting in HL-60 cells. Toxicol Vitro 2020;62:104667.

[43] Dell'Eva R, Ambrosini C, Vannini N, Piaggio G, Albini A, Ferrari N. AKT/NF-kappaB inhibitor xanthohumol targets cell growth and angiogenesis in hematologic malignancies. Cancer 2007;110:2007–11.

[44] Diller RA, Riepl HM, Rose O, Frias C, Henze G, Prokop A. Synthesis of demethylxanthohumol, a new potent apoptosis-inducing agent from hops. Chem Biodivers 2005;2:1331–7.

[45] Tronina T, Bartmanska A, Poplonski J, Rychlicka M, Sordon S, Filip-Psurska B, et al. Prenylated flavonoids with selective toxicity against human cancers. Int J Mol Sci 2023; 24.

[46] Grudzien M, Pawlak A, Tronina T, Kutkowska J, Kruszynska A, Poplonski J, et al. The effect of xanthohumol derivatives on apoptosis induction in canine lymphoma and leukemia cell lines. Int J Mol Sci 2023;24.

[47] Mi X, Wang C, Sun C, Chen X, Huo X, Zhang Y, et al. Xanthohumol induces paraptosis of leukemia cells through p38 mitogen activated protein kinase signaling pathway. Oncotarget 2017;8:31297–304.

[48] Wang CM, Chen J, Zhao J, Hu SS, Zhang SQ, Mi XQ, et al. Xanthohumol induces ROS through NADPH oxidase, causes cell cycle arrest and apoptosis. Oxid Med Cell Longev 2021; 2021:9877170.

[49] Luis C, Costa R, Rodrigues I, Castela A, Coelho P, Guerreiro S, et al. Xanthohumol and 8-prenylnaringenin reduce type 2 diabetes-associated oxidative stress by down-regulating galectin-3. Porto Biomed J 2019;4:e23.

[50] Xiao Y, Huang Z, Wang Y, Wang Y, Yu L, Yang J, et al. Xanthohumol attenuates collagen synthesis in scleroderma skin fibroblasts by ROS/Nrf2/TGFbeta1/Smad3 pathway. Eur J Pharmacol 2024;963:176227.

[51] Sun W, Yue J, Xu T, Cui Y, Huang D, Shi H, et al. Xanthohumol alleviates palmitate-induced inflammation and prevents osteoarthritis progression by attenuating mitochondria dysfunction/NLRP3 inflammasome axis. Heliyon 2023;9: e21282.

[52] Piasecki B, Biernasiuk A, Ludwiczuk A. Anti-coccal activity and composition of the essential oils and methanolic extracts obtained from brewing quality Humulus lupulus L. Hop pellets. Pharmaceuticals (Basel) 2023;16.

[53] Cheng W, Xu T, Cui L, Xue Z, Liu J, Yang R, et al. Discovery of amphiphilic xanthohumol derivatives as membrane-targeting antimicrobials against methicillin-resistant Staphylococcus aureus. J Med Chem 2023;66:962–75.

[54] Hao J, Speers RA, Fan H, Deng Y, Dai Z. A review of cyclic and oxidative bitter derivatives of alpha, iso-alpha and beta-hop acids. J Am Soc Brew Chem 2020;78:89–102.

[55] Harish V, Haque E, Smiech M, Taniguchi H, Jamieson S, Tewari D, et al. Xanthohumol for human malignancies: chemistry, pharmacokinetics and molecular targets. Int J Mol Sci 2021;22.

[56] Nowak B, Pozniak B, Poplonski J, Bobak L, Matuszewska A, Kwiatkowska J, et al. Pharmacokinetics of xanthohumol in rats of both sexes after oral and intravenous administration of pure xanthohumol and prenylflavonoid extract. Adv Clin Exp Med 2020;29:1101–9.

[57] Zugravu CA, Bohiltea RE, Salmen T, Pogurschi E, Otelea MR. Antioxidants in hops: bioavailability, health effects and perspectives for new products. Antioxidants (Basel) 2022;11.

[58] Andrusiak J, Mylkie K, Wysocka M, Scianowski J, Wolan A, Budny M. Synthesis of xanthohumol and xanthohumol-d(3) from naringenin. RSC Adv 2021;11:28934–9.

[59] Yang S, Chen R, Cao X, Wang G, Zhou YJ. De novo biosynthesis of the hops bioactive flavonoid xanthohumol in yeast. Nat Commun 2024;15:253.

[60] Awouafack MD, Lee Y-E, HJHoDF Morita. Xanthohumol: recent advances on resources, biosynthesis, bioavailability and pharmacology: biosynthesis pathway and. Pharmacology 2023:1–23.

[61] Xiao Q, Li Z, Miao Y, Xia J, Wu M. Editorial: prodrug design and therapeutic applications. Front Pharmacol 2023;14: 1280190.

[62] Oledzka E. Xanthohumol-A miracle molecule with biological activities: a review of biodegradable polymeric carriers and naturally derived compounds for its delivery. Int J Mol Sci 2024;25.

[63] Alalwany RH, Hawtrey T, Morgan K, Morris JC, Donaldson LF, Bates DO. Vascular endothelial growth factor isoforms differentially protect neurons against neurotoxic events associated with Alzheimer's disease. Front Mol Neurosci 2023;16:1181626.

[64] Batson J, Toop HD, Redondo C, Babaei-Jadidi R, Chaikuad A, Wearmouth SF, et al. Development of potent, selective SRPK1 inhibitors as potential topical therapeutics for neovascular eye disease. ACS Chem Biol 2017;12:825–32.

[65] Han X, Yang J, Jia Z, Wei P, Zhang H, Lv W, et al. Knockdown of serine-arginine protein kinase 1 inhibits the growth and migration in renal cell carcinoma cells. Oncol Res 2017; 25:389–95.

[66] Lima-Fontes M, Costa R, Rodrigues I, Soares R. Xanthohumol restores hepatic glucolipid metabolism balance in type 1 diabetic wistar rats. J Agric Food Chem 2017;65:7433–9.

[67] Amanitis D, Shahtaheri S, McWilliams DF, Walsh DA, Donaldson LF. Changes in the vascular endothelial growth factor A splicing AXIS in human synovium are related to arthritis pain. Osteoarthritis Cartilage 2021;29:S83-S.

[68] Yang SN, Zhong LY, Sun YH, Wang C, Ru WJ, Liu RZ, et al. Downregulation of lncRNA SNHG16 inhibits vascular smooth muscle cell proliferation and migration in cerebral atherosclerosis by targeting the miR-30c-5p/SDC2 axis. Heart Ves 2022;37:1085–96.

[69] Yao Y, Wang H, Xi X, Sun W, Ge J, Li P. miR-150 and SRPK1 regulate AKT3 expression to participate in LPS-induced inflammatory response. Innate Immun 2021;27:343–50.

[70] Liang X, Xu C, Wang W, Wang D, Zhu Y, Zhuang W, et al. Clinicopathologic characteristics and outcomes of East Asian patients with non-small-cell lung cancer and FLT3 mutations. J Thorac Oncol 2021;16:S563–S.

[71] Hasegawa H, Taniguchi H, Nakamura Y, Kato T, Fujii S, Ebi H, et al. FMS-like tyrosine kinase 3 (FLT3) amplification in patients with metastatic colorectal cancer. Cancer Sci 2021; 112:314–22.